

Response adjustable performance of a visco-elastomer sandwich plate with harmonic parameters and distributed supported masses under random loading

Measurement and Control
2022, Vol. 55(7-8) 631–645
© The Author(s) 2022
Article reuse guidelines:
sagepub.com/journals-permissions
DOI: 10.1177/00202940221105086
journals.sagepub.com/home/mac
 SAGE

Zhi-Gang Ruan¹, Zu-Guang Ying¹ and Yi-Qing Ni²

Abstract

Vibration control of composite structures with distributed masses under random loadings is a significant issue. Adjustability of dynamic characteristics including response spectrum peaks and valleys is important for structural vibration control. The vibration control design in space contains structure and conformation designs which combination results in periodic composite structures. In the present paper, spatial periodicity control design is proposed. Stochastic response adjustable performance of a visco-elastomer sandwich plate with harmonic distribution of geometrical and physical parameters and distributed supported masses under random base motion loading is studied. Both facial layer thickness and core layer modulus of the sandwich plate are considered as harmonic distribution in length and width directions as well as periodically distributed masses. Partial differential equations of coupling motions of the sandwich plate system are derived and converted into ordinary differential equations for multi-mode coupling vibration. Generalized stiffness, damping, and mass coefficients are functions of the harmonic distribution parameters. An analysis solution with frequency response function and response spectral density expressions of the sandwich plate system is obtained. Numerical results are given to show the response adjustable performance through the harmonic geometrical and physical parameters and distributed masses. The results have a potential application to stochastic vibration control or dynamic optimization design of smart composite structure systems.

Keywords

Random vibration, sandwich plate, harmonic distribution parameters, visco-elastomer core, distributed supported masses, analysis solution, response spectrum

Date received: 12 August 2021; accepted: 15 May 2022

Introduction

Structural vibration control, especially stochastic vibration control is an important research subject in engineering.^{1,2} For example, the vibration control of a system in which vibration-sensitive instruments are supported on base structure has been presented.³ Complex environmental disturbances are regarded as random loadings. The vibration control can be designed in time domain and in space. Most researches are on the temporal control design^{1,2,4–8} while relatively fewest researches are on the spatial control design. In terms of structure, to effectively attenuate vibration, damping sandwich structures are designed and studied increasingly. Sandwich beam and plate with distributed supported masses have been presented to model the

system in which vibration-sensitive instruments are supported on a planar structure.³ Vibration suppression effectiveness of a sandwich structure with non-adjustable viscoelastic core is limited under various loadings. Then controllable smart materials such as

¹Department of Mechanics, School of Aeronautics and Astronautics, Zhejiang University, Hangzhou, Zhejiang, China

²Hong Kong Branch of National Rail Transit Electrification and Automation Engineering Technology Research Center, Department of Civil and Environmental Engineering, The Hong Kong Polytechnic University, Kowloon Hong Kong, China

Corresponding author:

Zu-Guang Ying, Department of Mechanics, School of Aeronautics and Astronautics, Zhejiang University, Hangzhou, Zhejiang 310027, China.
Email: yingzg@zju.edu.cn



magneto-rheological (MR) liquid have been used as the core of a sandwich structure to provide adjustable dynamic properties,^{9–14} which can rapidly change in rheological properties under applied magnetic fields in millisecond.^{15–18} However, the MR liquid has certain instability such as magnetic particle settlement. Therefore, MR visco-elastomer (MRVE) has been developed to replace the MR liquid as the core of sandwich structures for effective vibration control.^{19–27}

In past decades, many researches were reported on dynamic characteristics and application to control devices of controllable MR liquid^{15–18} and MRVE.^{28–40} One-dimensional sandwich beam with MRVE core has been studied on periodic vibration and adjustable dynamic rigidity,^{19,20} frequency response characteristics,^{21–23} stochastic vibration response,²⁴ dynamic stability,^{25–27} and potential application.⁴¹ Furthermore, some researches on two-dimensional sandwich plate with MRVE core have been presented including vibration characteristics,^{42–45} sound transmission properties,⁴⁶ stochastic vibration response,⁴⁷ optimum location of partial core,^{48,49} and dynamic stability.^{50,51} However, in those researches, the MRVE core of sandwich beam and plate was only considered as having fully uniform or locally uniform mechanical properties. Therefore, to fully use MRVE controllability in space, the sandwich beam and plate with non-uniform or periodic dynamic properties of MRVE core need to be studied further. In this case, structural physical parameters are spatially non-uniform or periodic and thus, its vibration control differs from those researches.

In terms of conformation, periodic structures with spatially periodic distribution parameters have special dynamic characteristics, which have been studied on characteristic frequencies,^{52–60} modal localization and buckling,^{61–64} quasi-periodic distribution parameter effects^{65–73} and control application^{74–86} based on transfer matrix method, spatial harmonic expansion method, and finite element method, etc.^{87–93} However, the periodicity design has not been applied, but can be applied to improve composite structure dynamics. Therefore, periodic sandwich structure with MRVE core needs to be studied for dynamic optimization or vibration control. The periodic composite structure has MRVE dynamic properties adjustable by only applied magnetic fields while the structural design is unchanged, that can be as an active spatial periodicity control. Other geometrical periodicity design can be as passive spatial control. The active-passive spatial periodicity control is proposed in the present study. For the periodic composite structure, much more modes will be considered in analysis due to conventional vibration modes coupled with periodic distribution parameters. Its vibration equations are partial differential equations with space-varying parameters and random excitations, to which direct numerical solution is unsuitable for stochastic response statistics under various spatial parameters. Then analysis solution to the equations is an alternative. A periodic sandwich beam with MRVE core under

random loading has been studied, and results show its dynamic properties can be adjustable largely by periodic distribution parameters.⁹⁴ However, periodic sandwich plate with controllable visco-elastomer (VE) core (such as MRVE core) has not been studied and thus, needs to be studied further for dynamic optimization or vibration control of general two-dimensional structures.

In this paper, a class of controllable VEs such as MRVE is considered as the core of a sandwich plate. The VE sandwich plate with distributed supported masses is used for modeling a structural system in which vibration-sensitive instruments are supported on a planar structure. The VE sandwich plate is designed as spatially periodic for dynamic optimization or vibration control. The stochastic response characteristics of the sandwich plate with controllable VE core and distributed masses under random loading are studied, in which geometrical and physical parameters have harmonic distribution. First, both facial layer thickness and core layer modulus of the sandwich plate are considered as harmonic distribution in length and width directions. The masses are considered as periodic distribution on the plate. Second, partial differential equations for transverse and longitudinal coupling motions of the sandwich plate system are derived. Third, the equations are converted into coupling ordinary differential equations according to the Galerkin method. Fourth, an analysis solution with frequency response function and response spectral density expressions of the sandwich plate system is obtained based on random dynamics theory. Finally, numerical results are given to show the effects of the harmonic geometrical and physical parameters and distributed masses on stochastic response characteristics of the plate.

Vibration equations of sandwich plate with harmonic distribution parameters under random loading

A sandwich plate with controllable VE (or adjustable dynamics) core and supported concentrated masses is shown in Figure 1, where facial layer thickness and core layer modulus are spatial harmonic functions (in

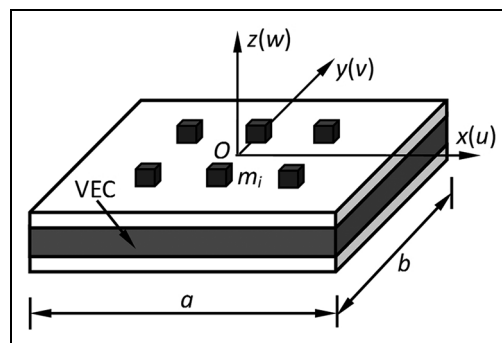


Figure 1. Sandwich plate with visco-elastomer core (VEC) and distributed masses.

coordinates x and y directions) and masses are distributed periodically. Length and width of the plate are a (direction x) and b (direction y), respectively. Two facial layers have identical Young's modulus E_1 , mass density ρ_1 and thickness h_1 . Middle core layer has mass density ρ_2 and thickness h_2 . The distributed masses are fixed on the plate. The i th distributed mass has mass $m_i \times ab$, while its size is very small compared with the plate length and width and thus is neglected. The sandwich plate is subjected to transverse base motion loading. The base has displacement w_0 which is a random loading.

The VE core has adjustable dynamic properties (e.g. MRVE has damping and stiffness adjustable by applied magnetic fields). The Young's modulus of the core layer is much smaller than that of the facial layers and thus is neglected. The shearing deformation is larger than that of the facial layers and needs to be considered. Based on viscoelastic dynamic stress-strain relation, shear stresses τ_{2xz} and τ_{2yz} of the core are expressed by the corresponding shear strain γ_{2xz} and γ_{2yz} as

$$\tau_{2xz} = G_{2a}\gamma_{2xz} + G_{2c}\frac{\partial\gamma_{2xz}}{\partial t} \quad (1)$$

$$\tau_{2yz} = G_{2a}\gamma_{2yz} + G_{2c}\frac{\partial\gamma_{2yz}}{\partial t} \quad (2)$$

where t is time variable, modulus parameters G_{2a} and G_{2c} are adjustable, for example, by applied magnetic fields. They vary harmonically with coordinates x and y , and are expressed as

$$G_{2a}(x, y) = e_{a1} + b_{a1} \cos \frac{2k_a \pi x}{a} \cos \frac{2k_b \pi y}{b} \quad (3)$$

$$G_{2c}(x, y) = e_{c1} + b_{c1} \cos \frac{2k_a \pi x}{a} \cos \frac{2k_b \pi y}{b} \quad (4)$$

where e_{a1} and e_{c1} are non-harmonic parts of the shear modulus parameters G_{2a} and G_{2c} , respectively, b_{a1} and b_{c1} are wave amplitudes of harmonic parts of the shear modulus parameters, k_a and k_b are wave numbers of harmonic parts of the shear modulus parameters. Thus, the shear modulus of the core is adjustable as actively spatial periodic design. The facial layer thickness is also designed to be varying harmonically with coordinates x and y , and is expressed as

$$h_1(x, y) = c_{1m} + b_{1r} \cos \frac{2k_1 \pi x}{a} \cos \frac{2k_2 \pi y}{b} \quad (5)$$

where c_{1m} is non-harmonic part of the thickness, b_{1r} is wave amplitude of harmonic part of the thickness, k_1 and k_2 are wave numbers of harmonic part of the thickness. Thus, the facial layer thickness is periodic as passively spatial design and needs to be optimized.

For the sandwich plate, it is assumed that (1) the facial layer materials are isotropic while the core

material is transversely isotropic, for example, under applied magnetic fields along z -axis; (2) normal stresses of the core layer are small and neglected; (3) normal stresses of the facial layers in z -axis direction are small and neglected; (4) transverse displacements of the sandwich plate are considered as invariant along the thickness; (5) a cross section of each facial layer is perpendicular to its axis line, and each cross section of the core layer is a plane in deformation; (6) longitudinal and rotational inertias of the plate are small and neglected; (7) interfaces between the facial layers and core layer are continuous all the time.^{47,95,96}

Based on the above assumptions, transverse plate displacement relative to base is $w = w(x, y, t)$. Horizontal displacements of upper and lower facial layers along x -axis and y -axis are expressed, respectively as

$$u_1(x, y, z_1, t) = u_{10}(x, y, t) - z_1 \frac{\partial w}{\partial x} \quad (6)$$

$$v_1(x, y, z_1, t) = v_{10}(x, y, t) - z_1 \frac{\partial w}{\partial y} \quad (7)$$

$$u_3(x, y, z_3, t) = u_{30}(x, y, t) - z_3 \frac{\partial w}{\partial x} \quad (8)$$

$$v_3(x, y, z_3, t) = v_{30}(x, y, t) - z_3 \frac{\partial w}{\partial y} \quad (9)$$

where u_{10} , v_{10} , u_{30} , and v_{30} are mid-layer displacements of the upper and lower facial layers, respectively, z_1 and z_3 are local transverse coordinates of the two facial layers. By using the displacements on upper and lower interfaces of the sandwich plate, shear strains of the core can be obtained as

$$\gamma_{2xz} = \frac{h_a}{h_2} \frac{\partial w}{\partial x} + \frac{u_{10} - u_{30}}{h_2} \quad (10)$$

$$\gamma_{2yz} = \frac{h_a}{h_2} \frac{\partial w}{\partial y} + \frac{v_{10} - v_{30}}{h_2} \quad (11)$$

where $h_a = h_1 + h_2$. Substituting strains (10) and (11) into expressions (1) and (2) yields the shear stresses of the core

$$\begin{aligned} \tau_{2xz} = & G_{2a} \left(\frac{h_a}{h_2} \frac{\partial w}{\partial x} + \frac{u_{10} - u_{30}}{h_2} \right) \\ & + G_{2c} \left[\frac{h_a}{h_2} \frac{\partial^2 w}{\partial x \partial t} + \frac{1}{h_2} \left(\frac{\partial u_{10}}{\partial t} - \frac{\partial u_{30}}{\partial t} \right) \right] \end{aligned} \quad (12)$$

$$\begin{aligned} \tau_{2yz} = & G_{2a} \left(\frac{h_a}{h_2} \frac{\partial w}{\partial y} + \frac{v_{10} - v_{30}}{h_2} \right) \\ & + G_{2c} \left[\frac{h_a}{h_2} \frac{\partial^2 w}{\partial y \partial t} + \frac{1}{h_2} \left(\frac{\partial v_{10}}{\partial t} - \frac{\partial v_{30}}{\partial t} \right) \right] \end{aligned} \quad (13)$$

Horizontal normal strains and shear strains of the upper and lower facial layers can be obtained using geometrical relations with displacements (6)–(9). The corresponding normal stresses and shear stresses are respectively

$$\sigma_{1x} = \frac{E_1}{1-\mu^2} \left[\left(\frac{\partial u_{10}}{\partial x} - z_1 \frac{\partial^2 w}{\partial x^2} \right) + \mu \left(\frac{\partial v_{10}}{\partial y} - z_1 \frac{\partial^2 w}{\partial y^2} \right) \right] \quad (14)$$

$$\sigma_{1y} = \frac{E_1}{1-\mu^2} \left[\left(\frac{\partial v_{10}}{\partial y} - z_1 \frac{\partial^2 w}{\partial y^2} \right) + \mu \left(\frac{\partial u_{10}}{\partial x} - z_1 \frac{\partial^2 w}{\partial x^2} \right) \right] \quad (15)$$

$$\tau_{1xy} = \frac{E_1}{2(1+\mu)} \left(\frac{\partial u_{10}}{\partial y} + \frac{\partial v_{10}}{\partial x} - 2z_1 \frac{\partial^2 w}{\partial x \partial y} \right) \quad (16)$$

$$\sigma_{3x} = \frac{E_1}{1-\mu^2} \left[\left(\frac{\partial u_{30}}{\partial x} - z_3 \frac{\partial^2 w}{\partial x^2} \right) + \mu \left(\frac{\partial v_{30}}{\partial y} - z_3 \frac{\partial^2 w}{\partial y^2} \right) \right] \quad (17)$$

$$\sigma_{3y} = \frac{E_1}{1-\mu^2} \left[\left(\frac{\partial v_{30}}{\partial y} - z_3 \frac{\partial^2 w}{\partial y^2} \right) + \mu \left(\frac{\partial u_{30}}{\partial x} - z_3 \frac{\partial^2 w}{\partial x^2} \right) \right] \quad (18)$$

$$\tau_{3xy} = \frac{E_1}{2(1+\mu)} \left(\frac{\partial u_{30}}{\partial y} + \frac{\partial v_{30}}{\partial x} - 2z_3 \frac{\partial^2 w}{\partial x \partial y} \right) \quad (19)$$

where μ is Poisson's ratio of the facial layers. By using equilibrium conditions in x and y directions with equations (14)–(19) and boundary conditions, the other shear stresses of the upper and lower facial layers are obtained as

$$\begin{aligned} \tau_{1xz} = & -\frac{E_1}{1-\mu^2} \left\{ \frac{\partial^2 u_{10}}{\partial x^2} \left(z_1 - \frac{h_1}{2} \right) + \frac{\partial^3 w}{\partial x^3} \left(\frac{h_1^2}{8} - \frac{z_1^2}{2} \right) \right. \\ & \left. + \mu \left[\frac{\partial^2 v_{10}}{\partial y \partial x} \left(z_1 - \frac{h_1}{2} \right) + \frac{\partial^3 w}{\partial y^2 \partial x} \left(\frac{h_1^2}{8} - \frac{z_1^2}{2} \right) \right] \right\} - \frac{E_1}{2(1+\mu)} \\ & \left[\frac{\partial^2 u_{10}}{\partial y^2} \left(z_1 - \frac{h_1}{2} \right) + \frac{\partial^2 v_{10}}{\partial y \partial x} \left(z_1 - \frac{h_1}{2} \right) + \frac{\partial^3 w}{\partial y^2 \partial x} \left(\frac{h_1^2}{4} - z_1^2 \right) \right] \end{aligned} \quad (20)$$

$$\begin{aligned} \tau_{1yz} = & -\frac{E_1}{1-\mu^2} \left\{ \frac{\partial^2 v_{10}}{\partial y^2} \left(z_1 - \frac{h_1}{2} \right) + \frac{\partial^3 w}{\partial y^3} \left(\frac{h_1^2}{8} - \frac{z_1^2}{2} \right) \right. \\ & \left. + \mu \left[\frac{\partial^2 u_{10}}{\partial y \partial x} \left(z_1 - \frac{h_1}{2} \right) + \frac{\partial^3 w}{\partial x^2 \partial y} \left(\frac{h_1^2}{8} - \frac{z_1^2}{2} \right) \right] \right\} \\ & - \frac{E_1}{2(1+\mu)} \left[\frac{\partial^2 v_{10}}{\partial x^2} \left(z_1 - \frac{h_1}{2} \right) + \frac{\partial^2 u_{10}}{\partial y \partial x} \left(z_1 - \frac{h_1}{2} \right) \right. \\ & \left. + \frac{\partial^3 w}{\partial x^2 \partial y} \left(\frac{h_1^2}{4} - z_1^2 \right) \right] \end{aligned} \quad (21)$$

$$\begin{aligned} \tau_{3xz} = & -\frac{E_1}{1-\mu^2} \left\{ \frac{\partial^2 u_{30}}{\partial x^2} \left(z_3 + \frac{h_1}{2} \right) + \frac{\partial^3 w}{\partial x^3} \left(\frac{h_1^2}{8} - \frac{z_3^2}{2} \right) \right. \\ & \left. + \mu \left[\frac{\partial^2 v_{30}}{\partial y \partial x} \left(z_3 + \frac{h_1}{2} \right) + \frac{\partial^3 w}{\partial y^2 \partial x} \left(\frac{h_1^2}{8} - \frac{z_3^2}{2} \right) \right] \right\} \\ & - \frac{E_1}{2(1+\mu)} \left[\frac{\partial^2 u_{30}}{\partial y^2} \left(z_3 + \frac{h_1}{2} \right) + \frac{\partial^2 v_{30}}{\partial y \partial x} \left(z_3 + \frac{h_1}{2} \right) \right. \\ & \left. + \frac{\partial^3 w}{\partial y^2 \partial x} \left(\frac{h_1^2}{4} - z_3^2 \right) \right] \end{aligned} \quad (22)$$

$$\begin{aligned} \tau_{3yz} = & -\frac{E_1}{1-\mu^2} \left\{ \frac{\partial^2 v_{30}}{\partial y^2} \left(z_3 + \frac{h_1}{2} \right) + \frac{\partial^3 w}{\partial y^3} \left(\frac{h_1^2}{8} - \frac{z_3^2}{2} \right) \right. \\ & \left. + \mu \left[\frac{\partial^2 u_{30}}{\partial y \partial x} \left(z_3 + \frac{h_1}{2} \right) + \frac{\partial^3 w}{\partial x^2 \partial y} \left(\frac{h_1^2}{8} - \frac{z_3^2}{2} \right) \right] \right\} \\ & - \frac{E_1}{2(1+\mu)} \left[\frac{\partial^2 v_{30}}{\partial x^2} \left(z_3 + \frac{h_1}{2} \right) \right. \\ & \left. + \frac{\partial^2 u_{30}}{\partial y \partial x} \left(z_3 + \frac{h_1}{2} \right) + \frac{\partial^3 w}{\partial x^2 \partial y} \left(\frac{h_1^2}{4} - z_3^2 \right) \right] \end{aligned} \quad (23)$$

Based on continuity conditions of the shear stresses on the interfaces between the facial layers and core layer of the sandwich plate, the differential equations for the longitudinal displacements are obtained as

$$\begin{aligned} \frac{E_1 h_1}{1-\mu^2} \left(\frac{\partial^2 u}{\partial x^2} + \mu \frac{\partial^2 v}{\partial y \partial x} \right) + \frac{E_1 h_1}{2(1+\mu)} \left(\frac{\partial^2 u}{\partial y^2} + \frac{\partial^2 v}{\partial y \partial x} \right) \\ = G_{2a} \left(\frac{h_a}{h_2} \frac{\partial w}{\partial x} + \frac{2}{h_2} u \right) + G_{2c} \left(\frac{h_a}{h_2} \frac{\partial^2 w}{\partial x \partial t} + \frac{2}{h_2} \frac{\partial u}{\partial t} \right) \end{aligned} \quad (24)$$

$$\begin{aligned} \frac{E_1 h_1}{1-\mu^2} \left(\frac{\partial^2 v}{\partial y^2} + \mu \frac{\partial^2 u}{\partial y \partial x} \right) + \frac{E_1 h_1}{2(1+\mu)} \left(\frac{\partial^2 v}{\partial x^2} + \frac{\partial^2 u}{\partial y \partial x} \right) \\ = G_{2a} \left(\frac{h_a}{h_2} \frac{\partial w}{\partial y} + \frac{2}{h_2} v \right) + G_{2c} \left(\frac{h_a}{h_2} \frac{\partial^2 w}{\partial y \partial t} + \frac{2}{h_2} \frac{\partial v}{\partial t} \right) \end{aligned} \quad (25)$$

where $u = u_{10} = -u_{30}$ and $v = v_{10} = -v_{30}$. The dynamic equation of the sandwich plate element with distributed masses in z direction is

$$\begin{aligned} \sum_{i=1}^3 \int_{-h_i/2}^{h_i/2} \left(\frac{\partial \tau_{ixz}}{\partial x} + \frac{\partial \tau_{iyz}}{\partial y} \right) dz_i \\ - \left[\rho h_t + \sum_{k=1}^{n_a} m_k a b \delta(x - x_k) \delta(y - y_k) \right] \\ \left(\frac{\partial^2 w}{\partial t^2} + \frac{\partial^2 w_0}{\partial t^2} \right) = 0 \end{aligned} \quad (26)$$

where $\delta(\cdot)$ is the Dirac delta function, n_a is total number of masses, (x_k, y_k) are coordinates of the k th mass, $\rho h_t = 2\rho h_1 + \rho h_2$ and $h_t = 2h_1 + h_2$. Substituting shear stresses (12), (13), and (20)–(23) into equation (26) yields the differential equation for the transverse displacement of the sandwich plate

$$\begin{aligned}
& \left[\rho h_t + \sum_{k=1}^{n_a} m_k ab \delta(x - x_k) \delta(y - y_k) \right] \frac{\partial^2 w}{\partial t^2} \\
& + D_1 \frac{\partial}{\partial x} \left[h_1^3 \left(\frac{\partial^3 w}{\partial x^3} + \frac{\partial^3 w}{\partial y^2 \partial x} \right) \right] + D_1 \frac{\partial}{\partial y} \left[h_1^3 \left(\frac{\partial^3 w}{\partial y^3} + \frac{\partial^3 w}{\partial x^2 \partial y} \right) \right] \\
& - \frac{\partial}{\partial x} \left[G_{2a} \frac{h_a^2}{h_2} \left(\frac{\partial w}{\partial x} + \frac{2u}{h_a} \right) + G_{2c} \frac{h_a^2}{h_2} \left(\frac{\partial^2 w}{\partial x \partial t} + \frac{2}{h_a} \frac{\partial u}{\partial t} \right) \right] \\
& - \frac{\partial}{\partial y} \left[G_{2a} \frac{h_a^2}{h_2} \left(\frac{\partial w}{\partial y} + \frac{2v}{h_a} \right) + G_{2c} \frac{h_a^2}{h_2} \left(\frac{\partial^2 w}{\partial y \partial t} + \frac{2}{h_a} \frac{\partial v}{\partial t} \right) \right] \\
& = - \left[\rho h_t + \sum_{k=1}^{n_a} m_k ab \delta(x - x_k) \delta(y - y_k) \right] \frac{\partial^2 w_0}{\partial t^2}
\end{aligned} \quad (27)$$

where $D_1 = E_1/6(1 - \mu^2)$. The partial differential equations (24), (25), and (27) describe coupled transverse and longitudinal motions of the VE sandwich plate with distributed masses under base loading, where coefficients are harmonic functions of coordinates x and y . Boundary conditions for various constrained sandwich plates have been given. The boundary conditions for simply supported rectangular plate are

$$\begin{aligned}
w|_{x=\pm a/2} = 0, \quad w|_{y=\pm b/2} = 0, \quad \frac{\partial^2 w}{\partial x^2}|_{x=\pm a/2} = 0, \\
\frac{\partial^2 w}{\partial y^2}|_{y=\pm b/2} = 0, \quad \left(\frac{\partial u}{\partial x} + \mu \frac{\partial v}{\partial y} \right)|_{x=\pm a/2} = 0, \\
\left(\frac{\partial v}{\partial y} + \mu \frac{\partial u}{\partial x} \right)|_{y=\pm b/2} = 0
\end{aligned} \quad (28)$$

Introduce non-dimensional (ND) coordinates and displacements as follows

$$\begin{aligned}
\bar{x} = \frac{x}{a}, \quad \bar{y} = \frac{y}{b}, \quad \bar{x}_k = \frac{x_k}{a}, \quad \bar{y}_k = \frac{y_k}{b}, \quad \bar{u} = \frac{u}{w_a}, \\
\bar{v} = \frac{v}{w_a}, \quad \bar{w} = \frac{w}{w_a}, \quad \bar{w}_0 = \frac{w_0}{w_a}
\end{aligned} \quad (29)$$

where w_a is amplitude of the base motion w_0 . The differential equations (27), (24), (25), and the boundary conditions (28) become

$$\begin{aligned}
& \left[\rho h_t + \sum_{k=1}^{n_a} m_k \delta(\bar{x} - \bar{x}_k) \delta(\bar{y} - \bar{y}_k) \right] \frac{\partial^2 \bar{w}}{\partial t^2} \\
& + D_1 \frac{\partial}{\partial \bar{x}} \left[\frac{h_1^3}{a^4} \left(\frac{\partial^3 \bar{w}}{\partial \bar{x}^3} + \frac{a^2}{b^2} \frac{\partial^3 \bar{w}}{\partial \bar{y}^2 \partial \bar{x}} \right) \right] \\
& + D_1 \frac{\partial}{\partial \bar{y}} \left[\frac{h_1^3}{b^4} \left(\frac{\partial^3 \bar{w}}{\partial \bar{y}^3} + \frac{b^2}{a^2} \frac{\partial^3 \bar{w}}{\partial \bar{x}^2 \partial \bar{y}} \right) \right] - \frac{\partial}{\partial \bar{x}} \\
& \left[G_{2a} \frac{h_a^2}{a^2 h_2} \left(\frac{\partial \bar{w}}{\partial \bar{x}} + \frac{2a\bar{u}}{h_a} \right) + G_{2c} \frac{h_a^2}{a^2 h_2} \left(\frac{\partial^2 \bar{w}}{\partial \bar{x} \partial t} + \frac{2a}{h_a} \frac{\partial \bar{u}}{\partial t} \right) \right] \\
& - \frac{\partial}{\partial \bar{y}} \left[G_{2a} \frac{h_a^2}{b^2 h_2} \left(\frac{\partial \bar{w}}{\partial \bar{y}} + \frac{2b\bar{v}}{h_a} \right) + G_{2c} \frac{h_a^2}{b^2 h_2} \left(\frac{\partial^2 \bar{w}}{\partial \bar{y} \partial t} + \frac{2b}{h_a} \frac{\partial \bar{v}}{\partial t} \right) \right] \\
& = - \left[\rho h_t + \sum_{k=1}^{n_a} m_k \delta(\bar{x} - \bar{x}_k) \delta(\bar{y} - \bar{y}_k) \right] \frac{\partial^2 \bar{w}_0}{\partial t^2}
\end{aligned} \quad (30)$$

$$\begin{aligned}
& 6D_1 h_1 \left(\frac{\partial^2 \bar{u}}{a^2 \partial \bar{x}^2} + \frac{1 - \mu}{2b^2} \frac{\partial^2 \bar{u}}{\partial \bar{y}^2} + \frac{1 + \mu}{2ab} \frac{\partial^2 \bar{v}}{\partial \bar{y} \partial \bar{x}} \right) \\
& = G_{2a} \left(\frac{h_a}{ah_2} \frac{\partial \bar{w}}{\partial \bar{x}} + \frac{2}{h_2} \bar{u} \right) + G_{2c} \left(\frac{h_a}{ah_2} \frac{\partial^2 \bar{w}}{\partial \bar{x} \partial t} + \frac{2}{h_2} \frac{\partial \bar{u}}{\partial t} \right)
\end{aligned} \quad (31)$$

$$\begin{aligned}
& 6D_1 h_1 \left(\frac{\partial^2 \bar{v}}{b^2 \partial \bar{y}^2} + \frac{1 - \mu}{2a^2} \frac{\partial^2 \bar{v}}{\partial \bar{x}^2} + \frac{1 + \mu}{2ab} \frac{\partial^2 \bar{u}}{\partial \bar{y} \partial \bar{x}} \right) \\
& = G_{2a} \left(\frac{h_a}{bh_2} \frac{\partial \bar{w}}{\partial \bar{y}} + \frac{2}{h_2} \bar{v} \right) + G_{2c} \left(\frac{h_a}{bh_2} \frac{\partial^2 \bar{w}}{\partial \bar{y} \partial t} + \frac{2}{h_2} \frac{\partial \bar{v}}{\partial t} \right)
\end{aligned} \quad (32)$$

$$\begin{aligned}
& \bar{w}|_{\bar{x}=\pm 1/2} = 0, \quad \bar{w}|_{\bar{y}=\pm 1/2} = 0, \quad \frac{\partial^2 \bar{w}}{\partial \bar{x}^2}|_{\bar{x}=\pm 1/2} = 0, \\
& \frac{\partial^2 \bar{w}}{\partial \bar{y}^2}|_{\bar{y}=\pm 1/2} = 0, \quad \left(\frac{\partial \bar{u}}{\partial \bar{x}} + \mu \frac{\partial \bar{v}}{\partial \bar{y}} \right)|_{\bar{x}=\pm 1/2} = 0, \\
& \left(\frac{\partial \bar{v}}{\partial \bar{y}} + \mu \frac{\partial \bar{u}}{\partial \bar{x}} \right)|_{\bar{y}=\pm 1/2} = 0
\end{aligned} \quad (33)$$

Stochastic response analysis of periodic sandwich plate

Based on the homogeneous boundary conditions (33), the ND vibration displacements of the sandwich plate can be expanded as

$$\bar{u} = \sum_{i=1}^{N_1} \sum_{j=1}^{N_2} r_{ij}(t) \sin[(2i-1)\pi\bar{x}] \cos[(2j-1)\pi\bar{y}] \quad (34)$$

$$\bar{v} = \sum_{i=1}^{N_1} \sum_{j=1}^{N_2} s_{ij}(t) \cos[(2i-1)\pi\bar{x}] \sin[(2j-1)\pi\bar{y}] \quad (35)$$

$$\bar{w} = \sum_{i=1}^{N_1} \sum_{j=1}^{N_2} q_{ij}(t) \cos[(2i-1)\pi\bar{x}] \cos[(2j-1)\pi\bar{y}] \quad (36)$$

where $r_{ij}(t)$, $s_{ij}(t)$, and $q_{ij}(t)$ are functions of time, N_1 and N_2 are integers. According to the Galerkin method, substituting displacements (34)–(36) into equations (30)–(32), multiplying the equations by $\cos[(2i-1)\pi\bar{x}] \cos[(2j-1)\pi\bar{y}]$, $\sin[(2i-1)\pi\bar{x}] \cos[(2j-1)\pi\bar{y}]$, and $\cos[(2i-1)\pi\bar{x}] \sin[(2j-1)\pi\bar{y}]$, respectively, and integrating them with respect to \bar{x} and \bar{y} yield ordinary differential equations for q_{ij} , r_{ij} , and s_{ij} . Note that the longitudinal velocity terms are relatively small. By eliminating functions r_{ij} and s_{ij} , the ordinary differential equations for q_{ij} can be obtained and rewritten in the matrix form

$$\mathbf{M} \frac{d^2 \mathbf{Q}}{dt^2} + \mathbf{C} \frac{d \mathbf{Q}}{dt} + \mathbf{K} \mathbf{Q} = \mathbf{F}(t) \quad (37)$$

where generalized excitation vector $\mathbf{F}(t) = -\mathbf{F}_C d^2 \bar{w}_0 / dt^2$, generalized displacement vector \mathbf{Q} , generalized mass matrix \mathbf{M} , generalized damping matrix \mathbf{C} , generalized stiffness matrix \mathbf{K} , and vector \mathbf{F}_C are

$$\mathbf{Q} = [\mathbf{Q}_1^T \mathbf{Q}_2^T \dots \mathbf{Q}_{N_2}^T]^T,$$

$$\mathbf{Q}_j = [q_{1j} \ q_{2j} \ \dots \ q_{N_{1j}}]^T$$

$$\mathbf{M} = \begin{bmatrix} \mathbf{M}_{11} & \mathbf{M}_{12} & \dots & \mathbf{M}_{1N_2} \\ \mathbf{M}_{21} & \mathbf{M}_{22} & \dots & \mathbf{M}_{2N_2} \\ \vdots & \vdots & \ddots & \vdots \\ \mathbf{M}_{N_2 1} & \mathbf{M}_{N_2 2} & \dots & \mathbf{M}_{N_2 N_2} \end{bmatrix},$$

$$\mathbf{M}_{jn} = \begin{bmatrix} M_{jn,11} & M_{jn,12} & \dots & M_{jn,1N_1} \\ M_{jn,21} & M_{jn,22} & \dots & M_{jn,2N_1} \\ \vdots & \vdots & \dots & \vdots \\ M_{jn,N_1 1} & M_{jn,N_1 2} & \dots & M_{jn,N_1 N_1} \end{bmatrix}$$

$$\mathbf{C} = \hat{\mathbf{C}} + \hat{\mathbf{C}}_{RS}, \quad \hat{\mathbf{C}}_{RS} = \mathbf{E} \mathbf{L}_{rv} + \mathbf{J} \mathbf{L}_{sv},$$

$$\mathbf{K} = \hat{\mathbf{K}} + \hat{\mathbf{K}}_{RS}, \quad \hat{\mathbf{K}}_{RS} = \mathbf{E} \mathbf{L}_{rd} + \mathbf{J} \mathbf{L}_{sd}$$

$$\mathbf{L}_{rv} = \mathbf{A}_a^{-1} \mathbf{B}_a (\mathbf{B}_b - \mathbf{A}_b \mathbf{A}_a^{-1} \mathbf{B}_a)^{-1} (\mathbf{V}_b - \mathbf{A}_b \mathbf{A}_a^{-1} \mathbf{V}_a) - \mathbf{A}_a^{-1} \mathbf{V}_a$$

$$\mathbf{L}_{rd} = \mathbf{A}_a^{-1} \mathbf{B}_a (\mathbf{B}_b - \mathbf{A}_b \mathbf{A}_a^{-1} \mathbf{B}_a)^{-1} (\mathbf{D}_b - \mathbf{A}_b \mathbf{A}_a^{-1} \mathbf{D}_a) - \mathbf{A}_a^{-1} \mathbf{D}_a$$

$$\mathbf{L}_{sv} = (\mathbf{B}_b - \mathbf{A}_b \mathbf{A}_a^{-1} \mathbf{B}_a)^{-1} (\mathbf{A}_b \mathbf{A}_a^{-1} \mathbf{V}_a - \mathbf{V}_b)$$

$$\mathbf{L}_{sd} = (\mathbf{B}_b - \mathbf{A}_b \mathbf{A}_a^{-1} \mathbf{B}_a)^{-1} (\mathbf{A}_b \mathbf{A}_a^{-1} \mathbf{D}_a - \mathbf{D}_b)$$

$$\hat{\mathbf{C}} = \begin{bmatrix} \hat{\mathbf{C}}_{11} & \hat{\mathbf{C}}_{12} & \dots & \hat{\mathbf{C}}_{1N_2} \\ \hat{\mathbf{C}}_{21} & \hat{\mathbf{C}}_{22} & \dots & \hat{\mathbf{C}}_{2N_2} \\ \vdots & \vdots & \ddots & \vdots \\ \hat{\mathbf{C}}_{N_2 1} & \hat{\mathbf{C}}_{N_2 2} & \dots & \hat{\mathbf{C}}_{N_2 N_2} \end{bmatrix},$$

$$\hat{\mathbf{C}}_{jn} = \begin{bmatrix} \hat{C}_{jn,11} & \hat{C}_{jn,12} & \dots & \hat{C}_{jn,1N_1} \\ \hat{C}_{jn,21} & \hat{C}_{jn,22} & \dots & \hat{C}_{jn,2N_1} \\ \vdots & \vdots & \dots & \vdots \\ \hat{C}_{jn,N_1 1} & \hat{C}_{jn,N_1 2} & \dots & \hat{C}_{jn,N_1 N_1} \end{bmatrix}$$

$$\hat{\mathbf{K}} = \begin{bmatrix} \hat{\mathbf{K}}_{11} & \hat{\mathbf{K}}_{12} & \dots & \hat{\mathbf{K}}_{1N_2} \\ \hat{\mathbf{K}}_{21} & \hat{\mathbf{K}}_{22} & \dots & \hat{\mathbf{K}}_{2N_2} \\ \vdots & \vdots & \ddots & \vdots \\ \hat{\mathbf{K}}_{N_2 1} & \hat{\mathbf{K}}_{N_2 2} & \dots & \hat{\mathbf{K}}_{N_2 N_2} \end{bmatrix},$$

$$\hat{\mathbf{K}}_{jn} = \begin{bmatrix} \hat{K}_{jn,11} & \hat{K}_{jn,12} & \dots & \hat{K}_{jn,1N_1} \\ \hat{K}_{jn,21} & \hat{K}_{jn,22} & \dots & \hat{K}_{jn,2N_1} \\ \vdots & \vdots & \dots & \vdots \\ \hat{K}_{jn,N_1 1} & \hat{K}_{jn,N_1 2} & \dots & \hat{K}_{jn,N_1 N_1} \end{bmatrix}$$

$$\mathbf{E} = \begin{bmatrix} \mathbf{E}_{11} & \mathbf{E}_{12} & \dots & \mathbf{E}_{1N_2} \\ \mathbf{E}_{21} & \mathbf{E}_{22} & \dots & \mathbf{E}_{2N_2} \\ \vdots & \vdots & \ddots & \vdots \\ \mathbf{E}_{N_2 1} & \mathbf{E}_{N_2 2} & \dots & \mathbf{E}_{N_2 N_2} \end{bmatrix},$$

$$\mathbf{E}_{jn} = \begin{bmatrix} E_{jn,11} & E_{jn,12} & \dots & E_{jn,1N_1} \\ E_{jn,21} & E_{jn,22} & \dots & E_{jn,2N_1} \\ \vdots & \vdots & \ddots & \vdots \\ E_{jn,N_1 1} & E_{jn,N_1 2} & \dots & E_{jn,N_1 N_1} \end{bmatrix}$$

$$\mathbf{J} = \begin{bmatrix} \mathbf{J}_{11} & \mathbf{J}_{12} & \dots & \mathbf{J}_{1N_2} \\ \mathbf{J}_{21} & \mathbf{J}_{22} & \dots & \mathbf{J}_{2N_2} \\ \vdots & \vdots & \ddots & \vdots \\ \mathbf{J}_{N_2 1} & \mathbf{J}_{N_2 2} & \dots & \mathbf{J}_{N_2 N_2} \end{bmatrix},$$

$$\mathbf{J}_{jn} = \begin{bmatrix} J_{jn,11} & J_{jn,12} & \dots & J_{jn,1N_1} \\ J_{jn,21} & J_{jn,22} & \dots & J_{jn,2N_1} \\ \vdots & \vdots & \ddots & \vdots \\ J_{jn,N_1 1} & J_{jn,N_1 2} & \dots & J_{jn,N_1 N_1} \end{bmatrix}$$

$$\mathbf{A}_\alpha = \begin{bmatrix} \mathbf{A}_{\alpha,11} & \mathbf{A}_{\alpha,12} & \dots & \mathbf{A}_{\alpha,1N_2} \\ \mathbf{A}_{\alpha,21} & \mathbf{A}_{\alpha,22} & \dots & \mathbf{A}_{\alpha,2N_2} \\ \vdots & \vdots & \ddots & \vdots \\ \mathbf{A}_{\alpha,N_2 1} & \mathbf{A}_{\alpha,N_2 2} & \dots & \mathbf{A}_{\alpha,N_2 N_2} \end{bmatrix},$$

$$\mathbf{A}_{\alpha,jn} = \begin{bmatrix} A_{\alpha,jn,11} & A_{\alpha,jn,12} & \dots & A_{\alpha,jn,1N_1} \\ A_{\alpha,jn,21} & A_{\alpha,jn,22} & \dots & A_{\alpha,jn,2N_1} \\ \vdots & \vdots & \ddots & \vdots \\ A_{\alpha,jn,N_1 1} & A_{\alpha,jn,N_1 2} & \dots & A_{\alpha,jn,N_1 N_1} \end{bmatrix}$$

$$\mathbf{B}_\alpha = \begin{bmatrix} \mathbf{B}_{\alpha,11} & \mathbf{B}_{\alpha,12} & \dots & \mathbf{B}_{\alpha,1N_2} \\ \mathbf{B}_{\alpha,21} & \mathbf{B}_{\alpha,22} & \dots & \mathbf{B}_{\alpha,2N_2} \\ \vdots & \vdots & \ddots & \vdots \\ \mathbf{B}_{\alpha,N_2 1} & \mathbf{B}_{\alpha,N_2 2} & \dots & \mathbf{B}_{\alpha,N_2 N_2} \end{bmatrix},$$

$$\mathbf{B}_{\alpha,jn} = \begin{bmatrix} B_{\alpha,jn,11} & B_{\alpha,jn,12} & \dots & B_{\alpha,jn,1N_1} \\ B_{\alpha,jn,21} & B_{\alpha,jn,22} & \dots & B_{\alpha,jn,2N_1} \\ \vdots & \vdots & \ddots & \vdots \\ B_{\alpha,jn,N_1 1} & B_{\alpha,jn,N_1 2} & \dots & B_{\alpha,jn,N_1 N_1} \end{bmatrix}$$

$$\mathbf{D}_\alpha = \begin{bmatrix} \mathbf{D}_{\alpha,11} & \mathbf{D}_{\alpha,12} & \dots & \mathbf{D}_{\alpha,1N_2} \\ \mathbf{D}_{\alpha,21} & \mathbf{D}_{\alpha,22} & \dots & \mathbf{D}_{\alpha,2N_2} \\ \vdots & \vdots & \ddots & \vdots \\ \mathbf{D}_{\alpha,N_2 1} & \mathbf{D}_{\alpha,N_2 2} & \dots & \mathbf{D}_{\alpha,N_2 N_2} \end{bmatrix},$$

$$\mathbf{D}_{\alpha,jn} = \begin{bmatrix} D_{\alpha,jn,11} & D_{\alpha,jn,12} & \dots & D_{\alpha,jn,1N_1} \\ D_{\alpha,jn,21} & D_{\alpha,jn,22} & \dots & D_{\alpha,jn,2N_1} \\ \vdots & \vdots & \ddots & \vdots \\ D_{\alpha,jn,N_1 1} & D_{\alpha,jn,N_1 2} & \dots & D_{\alpha,jn,N_1 N_1} \end{bmatrix}$$

$$\mathbf{V}_\alpha = \begin{bmatrix} \mathbf{V}_{\alpha,11} & \mathbf{V}_{\alpha,12} & \cdots & \mathbf{V}_{\alpha,1N_2} \\ \mathbf{V}_{\alpha,21} & \mathbf{V}_{\alpha,22} & \cdots & \mathbf{V}_{\alpha,2N_2} \\ \vdots & \vdots & \ddots & \vdots \\ \mathbf{V}_{\alpha,N_21} & \mathbf{V}_{\alpha,N_22} & \cdots & \mathbf{V}_{\alpha,N_2N_2} \end{bmatrix},$$

$$\mathbf{V}_{\alpha,jn} = \begin{bmatrix} V_{\alpha,jn,11} & V_{\alpha,jn,12} & \cdots & V_{\alpha,jn,1N_1} \\ V_{\alpha,jn,21} & V_{\alpha,jn,22} & \cdots & V_{\alpha,jn,2N_1} \\ \vdots & \vdots & \ddots & \vdots \\ V_{\alpha,jn,N_11} & V_{\alpha,jn,N_12} & \cdots & V_{\alpha,jn,N_1N_1} \end{bmatrix},$$

$$\alpha = a, b \quad (38)$$

Elements in the above matrices and vectors are determined by spatial integrals of coefficients in equations (30)–(32).

Equation (37) represents a stochastically excited multi-degree-of-freedom system derived from the sandwich plate with harmonic parameters and distributed masses under base loading. The system has the generalized mass, damping and stiffness dependent on harmonic distribution parameters k_1 , k_2 , k_a , k_b , b_{1r} , b_{a1} , and b_{c1} . Vibration response of the plate system can be estimated by using power spectral density function. Frequency response function and response spectral density matrices of the system (37) are obtained as

$$\mathbf{H}(\omega) = (\mathbf{K} + j\omega\mathbf{C} - \omega^2\mathbf{M})^{-1} \quad (39)$$

$$\mathbf{S}_Q(\omega) = \mathbf{H}(\omega)\mathbf{F}_C\mathbf{F}_C^T\mathbf{H}^*(\omega)\mathbf{S}_{\ddot{w}_0} \quad (40)$$

where ω is vibration frequency, $j = \sqrt{-1}$, superscript * denotes complex conjugate, $\mathbf{S}_{\ddot{w}_0}(\omega)$ is power spectral density of the base loading. By equations (36) and (40), spectral density function of the ND transverse displacement response of the plate is expressed as

$$S_{\bar{w}}(\omega, \bar{x}, \bar{y}) = \Phi^T(\bar{x}, \bar{y})\mathbf{S}_Q(\omega)\Phi(\bar{x}, \bar{y}) \quad (41)$$

where

$$\Phi(\bar{x}, \bar{y}) = [\Phi_1^T \quad \Phi_2^T \quad \cdots \quad \Phi_{N_2}^T]^T,$$

$$\Phi_j = [\varphi_{1j} \quad \varphi_{2j} \quad \cdots \quad \varphi_{N_1j}]^T \quad (42)$$

$$\varphi_{ij} = \cos[(2i-1)\pi\bar{x}] \cos[(2j-1)\pi\bar{y}]$$

Response statistics of the sandwich plate system subjected to random loading can be estimated using the spectral density function. For instance, the mean square displacement response of the plate is

$$E[\bar{w}^2(\bar{x}, \bar{y})] = \int_{-\infty}^{+\infty} S_{\bar{w}}(\omega, \bar{x}, \bar{y})d\omega \quad (43)$$

where $E[\cdot]$ denotes expectation operation of a stochastic process, which is equal to average over time domain for an ergodic stationary process. Based on the spectral density function (41), response characteristics of the sandwich plate adjustable by harmonic geometrical and physical parameters can be explored.

Numerical results and discussion

To show the response adjustable performance, consider a VE sandwich plate with harmonic parameters and distributed masses under base loading, which model a system with vibration-sensitive instruments supported on floor under random environmental disturbances.^{3,47} It has basic parameter values as follows: $a = 4\text{ m}$, $b = 2\text{ m}$, $\rho_1 = 3000\text{ kg/m}^3$, $\rho_2 = 1200\text{ kg/m}^3$, $E_1 = 10\text{ GPa}$, $\mu = 0.3$, $e_{a1} = 4\text{ MPa}$, $b_{a1} = \beta e_{a1}$, $e_{c1} = 0.006\text{ MPa}\cdot\text{s}$, $b_{c1} = \beta e_{c1}$, $c_{1m} = 0.05\text{ m}$, $b_{1r} = \alpha c_{1m}$, $h_2 = 0.2\text{ m}$, $n_a = 1$, $x_1 = y_1 = 0$, $m_1 = 240\text{ kg/m}^2$, $\alpha = 0.3$, $\beta = 0.5$, $w_a = 1$, and the loading is considered as white noise with power spectral density of 1.0×10^6 unless otherwise specified. Numbers N_1 and N_2 in expansion (36) are determined based on the convergence of displacement responses. Numerical results on stochastic responses and response spectral densities on the plate midpoint are shown in Figures 2–16.

Figure 2 shows that the root-mean-square (RMS) ND displacement (\bar{w}) responses of the sandwich plate ($b = 2, 2.5\text{ m}$) (distribution parameters $b_{1r} = 0$, $b_{a1} = 0$, $b_{c1} = 0$, $n_a = 1$) vary with the power spectral density of the ND base loading. The RMS displacement responses of the plate obtained by numerical simulation are also given, which validate the results obtained by the proposed analysis method. The numerical simulation is conducted as follows: samples of the random loading are firstly generated based on the power spectral density; stochastic responses

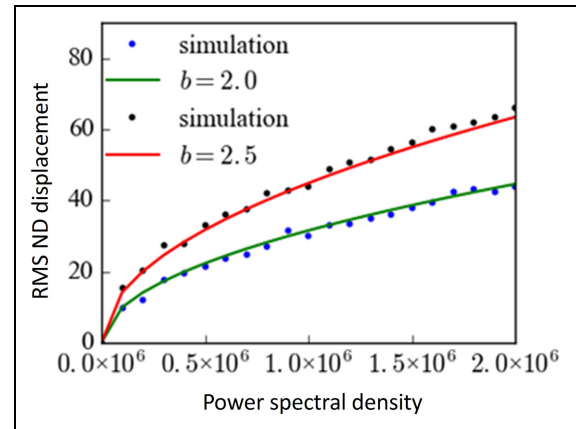


Figure 2. RMS ND displacement responses of the sandwich plate versus power spectral density of base loading.

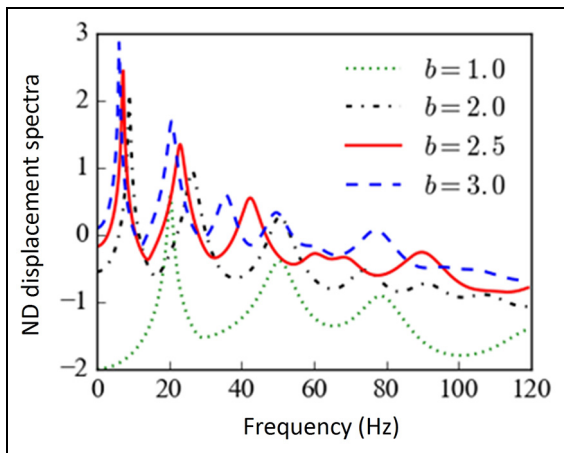


Figure 3. LND displacement response spectra of the sandwich plate for different plate widths b .

of the system (37) and plate (36) are calculated by using the Wilson-Theta algorithm; and then the response statistics are estimated.

Influence of sandwich plate width

The influence of the sandwich plate width on the ND displacement response spectra is considered ($\alpha = 0, \beta = 0$). Figure 3 shows the logarithmic ND (LND) displacement response spectra of the plate for different plate widths b . Many peaks and valleys can be seen, which indicate possible resonances and anti-resonances. As the plate width increases from 1.0 to 3.0 m, the first and second resonant frequencies decrease from 20.3 to 6.2 Hz and from 50.6 to 20.7 Hz, respectively. However, the first and second resonant response amplitudes increase from 3.75 to 729.7 and from 0.41 to 49.5 (non-logarithmic), respectively, as well as the anti-resonant response amplitudes. Thus, the width and length of the sandwich plate have large effects on the response characteristics and need to be determined suitably.

Influence of harmonic facial layer thickness

The influence of harmonic distribution of the facial layer thickness on the ND displacement response spectra of the sandwich plate is explored based on numerical results in Figures 4–8 ($\beta = 0$). Figure 4 shows the LND displacement spectra of the sandwich plate for different thickness wave numbers k_1 (in x direction) ($k_2 = 0.5, \alpha = 0.3$). The sandwich plate with harmonic thickness in multi-mode coupling vibration has multiple response resonances. The spectral peaks of the first, second, and third resonances of the harmonic plate are smaller than those of the non-harmonic plate ($b_{1r} = 0$), respectively (e.g. the non-logarithmic spectral amplitude of the first resonance is 124.9 for the non-harmonic plate, while the spectral amplitude of the first resonance is 86.2, 90.6, 103.5 for the harmonic plate with wave number $k_1 = 0.5, 0.8, 1.6$, respectively). Meanwhile, the wave number k_1 has certain effects on the resonant

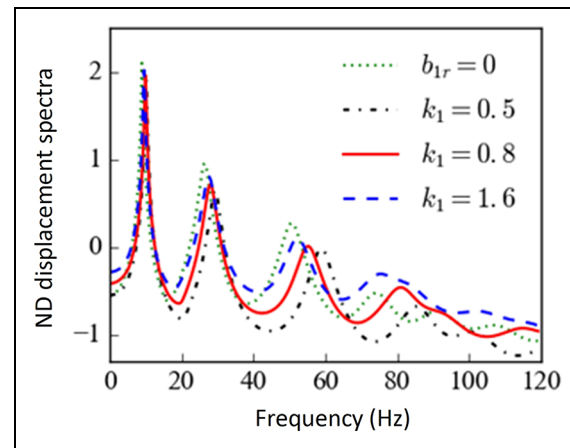


Figure 4. LND displacement response spectra of the sandwich plate for different thickness wave numbers k_1 .

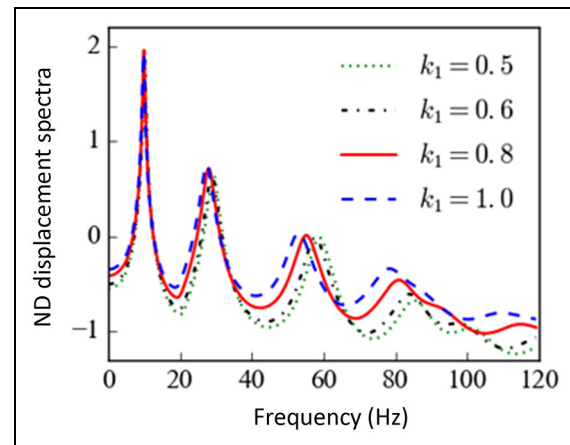


Figure 5. LND displacement response spectra of the sandwich plate for different thickness wave numbers k_1 .

frequencies, for example, the third resonant frequency of the harmonic sandwich plate is 58.9, 55.1, and 52.4 Hz for wave number $k_1 = 0.5, 0.8, 1.6$, respectively.

Figure 5 shows further the effects of the thickness wave number k_1 on the LND displacement response spectra of the sandwich plate. It is seen that the spectral peak of the first resonance has a minimum value (non-logarithmic 78.9) when the thickness wave number $k_1 \approx 0.6$. The spectral valley of the first anti-resonance has a minimum value when the thickness wave number $k_1 \approx 0.5$. Thus, the thickness wave number k_1 has large effects on the vibration response of the harmonic sandwich plate. The response has various adjustable performances in different vibration frequency bands by suitably choosing the wave number.

Figure 6 shows the LND displacement spectra of the sandwich plate for different thickness wave numbers k_2 (in y direction) ($k_1 = 0.5, \alpha = 0.3$). It is seen that the wave number k_2 similar to k_1 has large effects on the resonant response amplitudes and frequencies. For instance, the non-logarithmic spectral amplitude of the

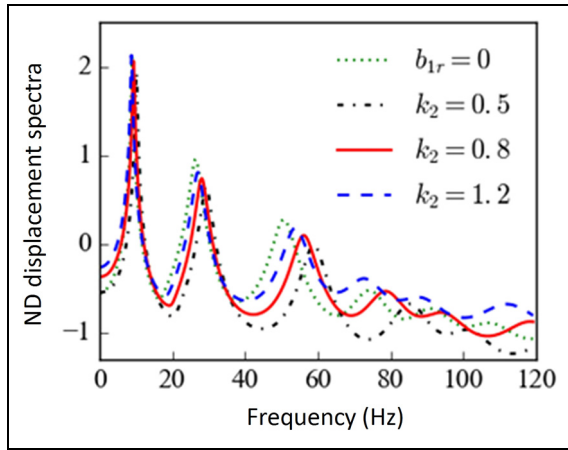


Figure 6. LND displacement response spectra of the sandwich plate for different thickness wave numbers k_2 .

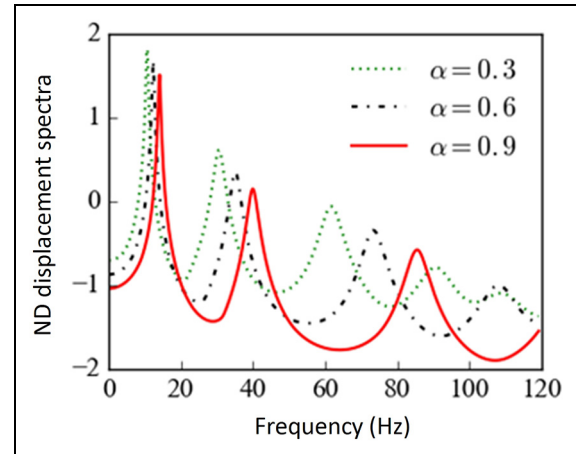


Figure 8. LND displacement response spectra of the sandwich plate for different parameters α .

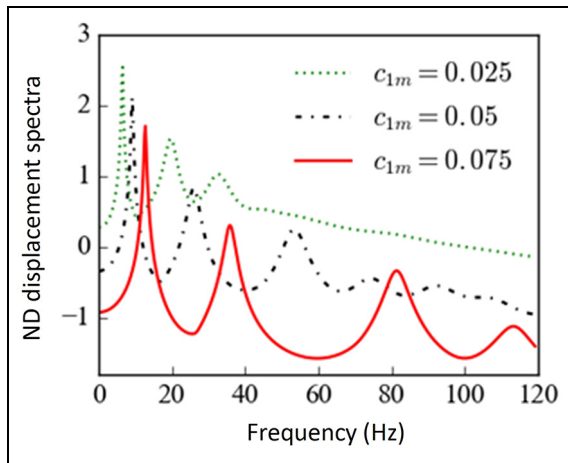


Figure 7. LND displacement response spectra of the sandwich plate for different non-periodic parts of the thicknesses c_{1m} .

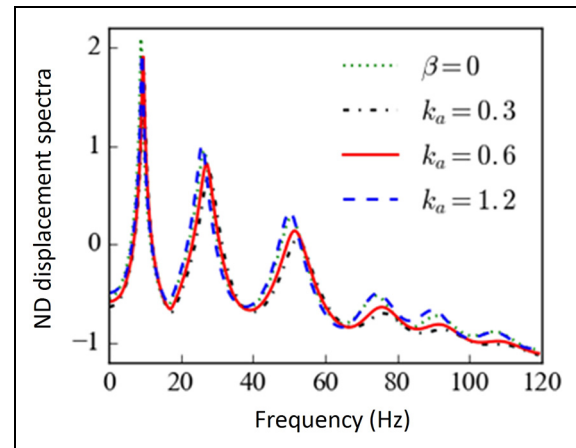


Figure 9. LND displacement response spectra of the sandwich plate for different modulus wave numbers k_a .

second resonance is 8.99 for the non-harmonic plate and 4.46, 5.48, 6.43 for the harmonic plate with wave number $k_2 = 0.5, 0.8, 1.2$, respectively. The spectral peaks of the first, second, and third resonances of the harmonic sandwich plate are smaller than those of the non-harmonic sandwich plate.

Figure 7 shows the LND displacement response spectra of the sandwich plate for different non-harmonic parts of the thickness c_{1m} ($k_1 = 2.8, k_2 = 0.8$). As the non-harmonic part c_{1m} increases, the spectral peaks and valleys of the first, second, and third resonances and anti-resonances decrease, while the first, second, and third resonance frequencies increase due to the plate stiffness increasing.

Figure 8 shows the LND displacement response spectra of the sandwich plate for different parameters α (ratio of harmonic part to non-harmonic part of the thickness) ($\beta = 0, k_1 = 0.4, k_2 = 0.3$). It is seen that the spectral peaks and valleys of the first, second, and third resonances and anti-resonances decrease, while the first, second and third resonant frequencies increase as the parameter α increases (e.g. the non-logarithmic spectral amplitude of the first resonance is 65.4, 48.3, 32.4, and the first resonant

frequency is 10.6, 12.3, and 14.1 Hz for the parameter $\alpha = 0.3, 0.6, 0.9$, respectively). The ratio of harmonic part to non-harmonic part of the thickness has large effects on the vibration response. Thus, the response has remarkable adjustable performance including resonant peaks and anti-resonant valleys by suitably choosing the wave amplitude or ratio of harmonic part to non-harmonic part.

Influence of harmonic core layer modulus

The influence of harmonic distribution of the core layer modulus on the ND displacement response spectra of the sandwich plate is explored based on numerical results in Figures 9–12 ($\alpha = 0$). Figure 9 shows the LND displacement spectra of the sandwich plate for different wave numbers of the modulus k_a (in x direction) ($k_b = 0.5, \beta = 0.5$). It is seen that the spectral peak of the first resonance of the harmonic plate is smaller than that of the non-harmonic plate ($\beta = 0$) (the non-logarithmic spectral amplitude of the first resonance is 124.9 for the non-harmonic plate, while the spectral amplitude of the first resonance is 67.2,

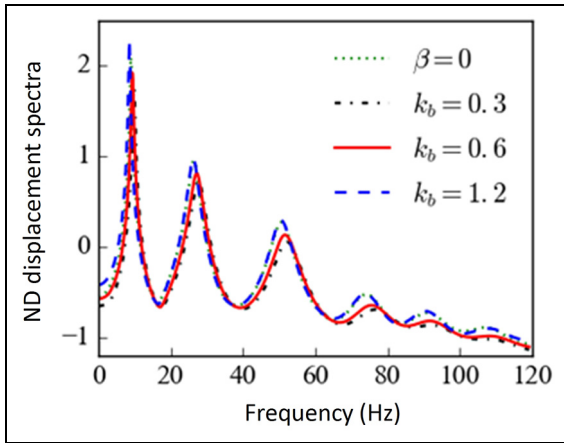


Figure 10. LND displacement response spectra of the sandwich plate for different modulus wave numbers k_b .

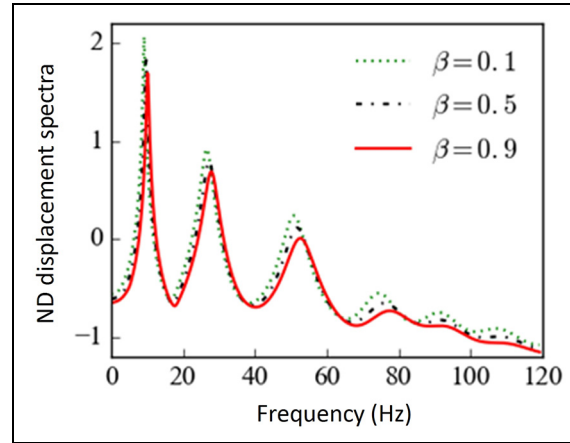


Figure 12. LND displacement response spectra of the sandwich plate for different parameters β .

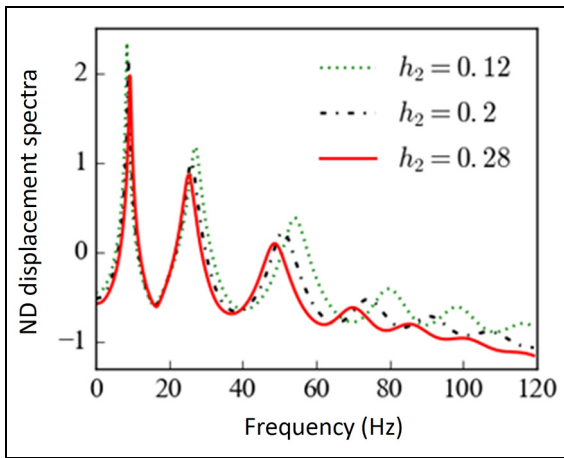


Figure 11. LND displacement response spectra of the sandwich plate for different core layer thicknesses h_2 .

80.4, 88.4 for the harmonic plate with wave number $k_a = 0.3, 0.6, 1.2$, respectively). The wave number k_a has certain effects on the resonant frequencies, for example, the third resonant frequency is 52.4, 51.6, and 50.2 Hz for wave number $k_a = 0.3, 0.6, 1.2$, respectively. The spectral peak or valley of the resonant or anti-resonant response has a minimum value for an optimum value of the wave number k_a . Similar results can be obtained by Figure 10 which shows the LND displacement spectra of the sandwich plate for different wave numbers of the modulus k_b (in y direction) ($k_a = 0.5, \beta = 0.5$). Thus, the wave numbers k_a and k_b of the modulus have large effects on the vibration response of the harmonic sandwich plate. The response has various adjustable performances in different vibration frequency bands by suitably choosing the wave numbers.

Figure 11 shows the LND displacement response spectra of the harmonic sandwich plate for different core layer thicknesses h_2 ($k_a = 3.6, k_b = 1.2, \beta = 0.5$). As the thickness h_2 increases, the spectral peaks of the first, second, and third resonances decrease, and the second and third resonance frequencies decrease.

Figure 12 shows the LND displacement response spectra of the sandwich plate for different parameters β

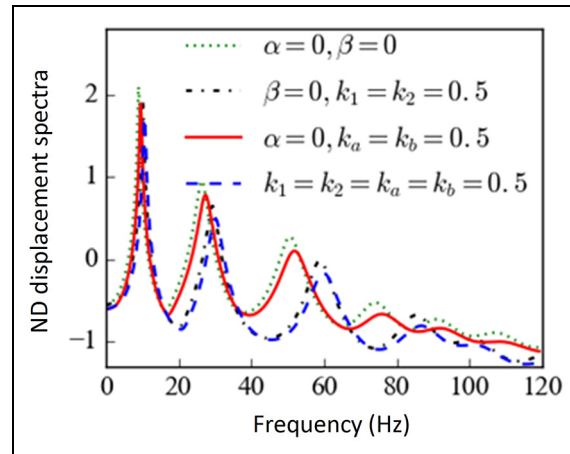


Figure 13. LND displacement response spectra of the sandwich plate for different wave amplitude ratios α and β .

(ratio of harmonic part to non-harmonic part of the modulus) ($\alpha = 0, k_a = 0.6, k_b = 0.4$). It is seen that the spectral peaks and valleys of the first, second and third resonances and anti-resonances decrease, while the first, second, and third resonant frequencies increase as the parameter β increases (e.g. the non-logarithmic spectral amplitude of the first resonance is 115.9, 66.6, 49.1, and the first resonant frequency is 9.2, 9.8, and 10.2 Hz for the parameter $\beta = 0.1, 0.5, 0.9$, respectively). The ratio of harmonic part to non-harmonic part of the modulus has large effects on the vibration response. Thus, the response has remarkable adjustable performance including resonant peaks and anti-resonant valleys by suitably choosing the wave amplitude or ratio of harmonic part to non-harmonic part.

Influence of both harmonic thickness and modulus

The influence of harmonic distribution of both the thickness and modulus on the ND displacement response spectra of the sandwich plate is further illustrated by numerical results in Figures 13 and 14 ($\alpha = 0.3, \beta = 0.5$). Figure 13 shows the LND

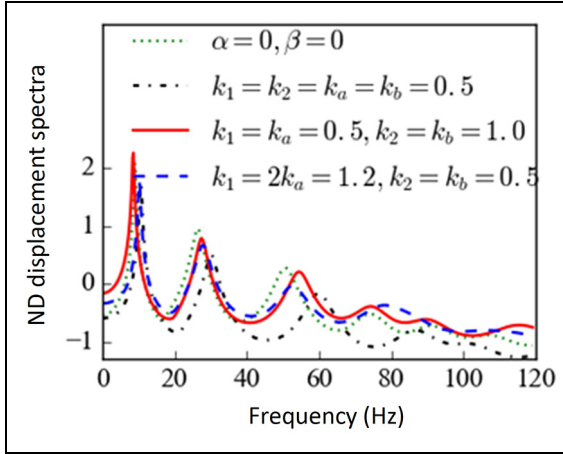


Figure 14. LND displacement response spectra of the sandwich plate for different wave numbers k_1 , k_2 , k_a and k_b .

displacement spectra of the sandwich plate for different wave amplitude ratios α and β ($k_1 = k_2 = k_a = k_b = 0.5$). The harmonic distribution of both the thickness and modulus ($\alpha = 0.3$, $\beta = 0.5$) can reduce the spectral peaks and valleys of the first, second, and third resonances and anti-resonances more than the harmonic distribution of only the thickness ($\alpha = 0.3$, $\beta = 0$) or only the modulus ($\alpha = 0$, $\beta = 0.5$) (e.g. the non-logarithmic spectral amplitude of the first resonance is 86.2, 77.6, 52.8 for only the harmonic modulus $\beta = 0.5$, only the harmonic thickness $\alpha = 0.3$, and both the harmonic thickness and modulus $\alpha = 0.3$, $\beta = 0.5$, respectively). Figure 14 shows the LND displacement spectra of the sandwich plate for different wave numbers k_1 , k_2 , k_a , and k_b . The suitable wave numbers of harmonic thickness and modulus can further improve the vibration response characteristics of the sandwich plate.

Influence of periodically distributed masses

The influence of distribution of supported masses on the displacement response spectra of the harmonic sandwich plate is also considered in five cases. Case A is only one mass (240 kg/m^2) on the plate with ND coordinates (0, 0). Case B is three equal masses (80 kg/m^2) on the plate with ND coordinates $(-0.25, 0)$, $(0, 0)$, $(0.25, 0)$, respectively. Case C is three equal mass (80 kg/m^2) on the plate with ND coordinates $(0, -0.25)$, $(0, 0)$, $(0, 0.25)$, respectively. Case D is five equal masses (48 kg/m^2) on the plate with ND coordinates $(-0.25, -0.25)$, $(-0.25, 0.25)$, $(0, 0)$, $(0.25, -0.25)$, $(0.25, 0.25)$, respectively. Case E is five equal mass (48 kg/m^2) on the plate with ND coordinates $(-0.25, 0)$, $(0, -0.25)$, $(0, 0)$, $(0, 0.25)$, $(0.25, 0)$, respectively. Numerical results on the ND displacement response spectra under different mass distributions are shown in Figures 15 and 16 ($k_1 = k_2 = k_a = k_b = 0.5$, $\alpha = 0.3$, $\beta = 0.5$).

Figure 15 shows the LND displacement spectra of the sandwich plate for distribution cases A, B, and D. It is seen that the mass decentralization (different

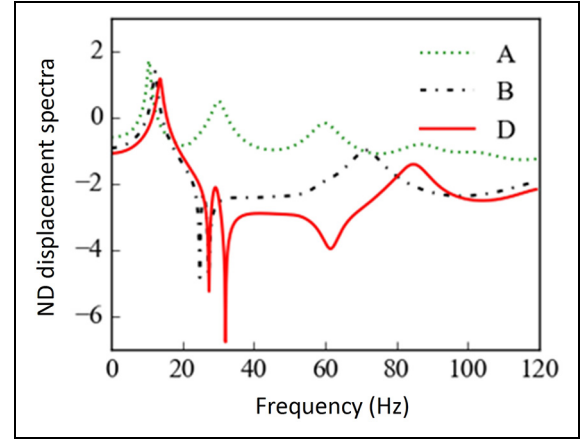


Figure 15. LND displacement response spectra of the sandwich plate with distributed masses for cases A, B and D.

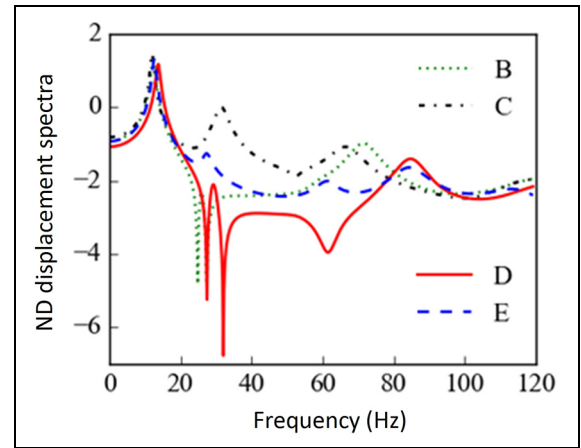


Figure 16. LND displacement response spectra of the sandwich plate with distributed masses for cases B, C, D, and E.

numbers of masses, but equal total mass) has large effects on the response spectrum including resonant peaks and anti-resonant valleys as well as resonant frequencies (e.g. the non-logarithmic spectral amplitude of the first resonance is 52.8, 24.7, 15.0, and the first resonant frequency is 10.5, 12.5, and 13.7 Hz for cases A, B, D, respectively). The mass decentralization can reduce the spectral peaks and valleys and then improve the vibration response characteristics of the harmonic sandwich plate.

Figure 16 shows the LND displacement spectra of the sandwich plate for distribution cases B, C, D, and E. It is seen that the suitable mass placement (equal number of masses, but different placements, e.g. B and C, D and E) can largely reduce the spectral peaks and valleys and then improve the vibration response characteristics. Thus, the response has remarkable adjustable performance including resonant peaks and anti-resonant valleys by suitable periodic distribution of masses supported on the harmonic sandwich plate.

Conclusions

The response adjustable performance of a visco-elastomer sandwich plate with harmonic geometrical and physical parameters and periodically distributed masses under random base motion loading has been studied for spatial periodicity control. The spatial harmonic distribution of facial layer thickness and core layer modulus of the sandwich plate is considered as well as the periodic distribution of the supported masses. The partial differential equations for transverse and longitudinal coupling motions of the sandwich plate with distributed masses under base loading are derived. The equations are further converted into multi-mode coupling vibration equations with stiffness, damping, and mass coefficients dependent on harmonic distribution parameters. The analysis solution to the equations is proposed, and the frequency response function and response spectral density expressions of the sandwich plate system are obtained, which are used for response adjustable performance analysis or dynamic optimization analysis of the periodic composite structure system.

Numerical results have demonstrated that: (1) the vibration response characteristics of the sandwich plate can be adjusted by plate width and length; (2) the vibration response characteristics of the sandwich plate can be improved largely by the harmonic distribution of geometrical and physical parameters, for example, the response amplitudes of resonances and anti-resonances can be remarkably reduced by suitably choosing wave numbers and wave amplitudes of the thickness and modulus; (3) the periodic mass distribution (decentralization and optimized placement) can largely improve the vibration response characteristics of the sandwich plate, including resonant and anti-resonant amplitudes. The results on response adjustable performance have a potential application to the stochastic vibration control or dynamic optimization design of smart composite structures with distributed masses through harmonic distribution of geometrical and physical parameters. However, an active temporal control strategy with the spatial periodicity strategy for the vibration control of visco-elastomer composite structures needs to be developed further.

Declaration of conflicting interests


The author(s) declared no potential conflicts of interest with respect to the research, authorship, and/or publication of this article.


Funding

The author(s) disclosed receipt of the following financial support for the research, authorship, and/or publication of this article: This research was funded by the National Natural Science Foundation of China (grant number 12072312), the Research Grants Council of the Hong Kong Special Administrative Region (grant number R-5020-18), and the

Innovation and Technology Commission of the Hong Kong Special Administrative Region (grant number K-BBY1).

ORCID iDs

Zu-Guang Ying  <https://orcid.org/0000-0003-1795-6968>

Yi-Qing Ni  <https://orcid.org/0000-0003-1527-7777>

References

1. Soong TT and Spencer BF. Supplemental energy dissipation: state-of-the-art and state-of-the-practice. *Eng Struct* 2002; 24: 243–259.
2. Spencer BF and Nagarajaiah S. State of the art of structural control. *ASCE J Struct Eng* 2003; 129: 845–856.
3. Ni YQ, Ying ZG and Chen ZH. Micro-vibration suppression of equipment supported on a floor incorporating magneto-rheological elastomer core. *J Sound Vib* 2011; 330: 4369–4383.
4. Mostafaei J, Mobayen S, Vaseghi B, et al. Complex dynamical behaviors of a novel exponential hyperchaotic system and its application in fast synchronization and color image encryption. *Sci Prog* 2021; 104: 368504211003388.
5. Vaseghi B, Mobayen S, Hashemi SS, et al. Fast reaching finite time synchronization approach for chaotic systems with application in medical image encryption. *IEEE Access* 2021; 9: 25911–25925.
6. Vaseghi B, Hashemi SS, Mobayen S, et al. Finite time chaos synchronization in time-delay channel and its application to satellite image encryption in OFDM communication systems. *IEEE Access* 2021; 9: 21332–21344.
7. Bauomy HS and EL-Sayed AT. Mixed controller (IRC + NSC) involved in the harmonic vibration response cantilever beam model. *Meas Control* 2020; 53: 1954–1967.
8. Enríquez-Zárate J, Abundis-Fong HF, Velázquez R, et al. Passive vibration control in a civil structure: experimental results. *Meas Control* 2019; 52: 938–946.
9. Fisco NR and Adeli H. Smart structures: part I—active and semi-active control. *Sci Iran* 2011; 18: 275–284.
10. Casciati F, Rodellar J and Yildirim U. Active and semi-active control of structures – theory and applications: a review of recent advances. *J Intell Mater Syst Struct* 2012; 23: 1181–1195.
11. Eshaghi M, Sedaghati R and Rakheja S. Dynamic characteristics and control of magnetorheological/electrorheological sandwich structures: a state-of-the-art review. *J Intell Mater Syst Struct* 2016; 27: 2003–2037.
12. Rajamohan V, Rakheja S and Sedaghati R. Vibration analysis of a partially treated multi-layer beam with magnetorheological fluid. *J Sound Vib* 2010; 329: 3451–3469.
13. Manoharan R, Vasudevan R and Jeevanantham AK. Dynamic characterization of a laminated composite magnetorheological fluid sandwich plate. *Smart Mater Struct* 2014; 23: 025022.
14. Asgari M, Rayyat Rokn-Abadi M, Yousefi M, et al. Aeroelastic analysis of a sandwich panel with partially treated magneto-rheological fluid core. *J Intell Mater Syst Struct* 2019; 30: 140–154.
15. Dyke SJ, Spencer BF, Sain MK, et al. Modeling and control of magnetorheological dampers for seismic response reduction. *Smart Mater Struct* 1996; 5: 565–575.

16. Wang DH and Liao WH. Magnetorheological fluid dampers: a review of parametric modelling. *Smart Mater Struct* 2011; 20: 023001.
17. Zhu X, Jing X and Cheng L. Magnetorheological fluid dampers: a review on structure design and analysis. *J Intell Mater Syst Struct* 2012; 23: 839–873.
18. Choi SB, Li W, Yu M, et al. State of the art of control schemes for smart systems featuring magneto-rheological materials. *Smart Mater Struct* 2016; 25: 043001.
19. Zhou GY and Wang Q. Magnetorheological elastomer-based smart sandwich beams with nonconductive skins. *Smart Mater Struct* 2005; 14: 1001–1009.
20. Zhou GY and Wang Q. Study on the adjustable rigidity of magnetorheological-elastomer-based sandwich beams. *Smart Mater Struct* 2006; 15: 59–74.
21. Choi WJ, Xiong YP and Shenoi RA. Vibration characteristics of sandwich beams with steel skins and magnetorheological elastomer cores. *Adv Struct Eng* 2010; 13: 837–847.
22. Bornassi S and Navazi HM. Torsional vibration analysis of a rotating tapered sandwich beam with magnetorheological elastomer core. *J Intell Mater Syst Struct* 2018; 29: 2406–2423.
23. Hu G, Guo M, Li W, et al. Experimental Investigation of the vibration characteristics of a magnetorheological elastomer sandwich beam under non-homogeneous small magnetic fields. *Smart Mater Struct* 2011; 20: 127001.
24. Ying ZG, Ni YQ and Huan RH. Stochastic microvibration response analysis of a magnetorheological viscoelastomer based sandwich beam under localized magnetic fields. *Appl Math Model* 2015; 39: 5559–5566.
25. Dwivedy SK, Mahendra N and Sahu KC. Parametric instability regions of a soft and magnetorheological elastomer cored sandwich beam. *J Sound Vib* 2009; 325: 686–704.
26. Nayak B, Dwivedy SK and Murthy KS. Dynamic stability of magnetorheological elastomer based adaptive sandwich beam with conductive skins using FEM and the harmonic balance method. *Int J Mech Sci* 2013; 77: 205–216.
27. Rokn-Abadi M, Yousefi M, Haddadpour H, et al. Dynamic stability analysis of a sandwich beam with magnetorheological elastomer core subjected to a follower force. *Acta Mech* 2020; 231: 3715–3727.
28. Shiga T, Okada A and Kurauchi T. Magnetorheological behavior of composite gels. *J Appl Polym Sci* 1995; 58: 787–792.
29. Jolly MR, Carlson JD, Muñoz BC, et al. The magnetorheological response of elastomer composites consisting of ferrous particles embedded in a polymer matrix. *J Intell Mater Syst Struct* 1996; 7: 613–622.
30. Ginder JM, Clark SM, Schlotter WF, et al. Magnetostrictive phenomena in magneto-rheological elastomers. *Int J Mod Phys B* 2002; 16: 2412–2418.
31. Bellan C and Bossis G. Field dependence of viscoelastic properties of MR elastomers. *Int J Mod Phys B* 2002; 16: 2447–2453.
32. Shen Y, Golnaraghi MF and Heppler GR. Experimental research and modeling of magnetorheological elastomers. *J Intell Mater Syst Struct* 2004; 15: 27–35.
33. Gong XL, Zhang XZ and Zhang PQ. Fabrication and characterization of isotropic magnetorheological elastomers. *Polym Test* 2005; 24: 669–676.
34. Böse H. Viscoelastic properties of silicone-based magnetorheological elastomers. *Int J Mod Phys B* 2007; 21: 4790–4797.
35. Kallio M, Lindroos T, Aalto S, et al. Dynamic compression testing of a tunable spring element consisting of a magnetorheological elastomer. *Smart Mater Struct* 2007; 16: 506–514.
36. Li Y, Li J, Li W, et al. A state-of-the-art review on magnetorheological elastomer devices. *Smart Mater Struct* 2014; 23: 123001.
37. York D, Wang X and Gordaninejad F. A new MR fluid-elastomer vibration isolator. *J Intell Mater Syst Struct* 2007; 18: 1221–1225.
38. Hu W and Wereley NM. Hybrid magnetorheological fluid–elastomeric lag dampers for helicopter stability augmentation. *Smart Mater Struct* 2008; 17: 045021.
39. Hoang N, Zhang N and Du H. An adaptive tunable vibration absorber using a new magnetorheological elastomer for vehicular powertrain transient vibration reduction. *Smart Mater Struct* 2011; 20: 015019.
40. Jung HJ, Eem SH, Jang DD, et al. Seismic performance analysis of a smart base-isolation system considering dynamics of MR elastomers. *J Intell Mater Syst Struct* 2011; 22: 1439–1450.
41. Ahamed R, Choi SB and Ferdaus MM. A state of art on magneto-rheological materials and their potential applications. *J Intell Mater Syst Struct* 2018; 29: 2051–2095.
42. Yeh JY. Vibration analysis of sandwich rectangular plates with magnetorheological elastomer damping treatment. *Smart Mater Struct* 2013; 22: 035010.
43. Aguib S, Nour A, Zahloul H, et al. Dynamic behavior analysis of a magnetorheological elastomer sandwich plate. *Int J Mech Sci* 2014; 87: 118–136.
44. Babu VR and Vasudevan R. Dynamic analysis of tapered laminated composite magnetorheological elastomer (MRE) sandwich plates. *Smart Mater Struct* 2016; 25: 035006.
45. Mikhasev GI, Eremeyev VA, Wilde K, et al. Assessment of dynamic characteristics of thin cylindrical sandwich panels with magnetorheological core. *J Intell Mater Syst Struct* 2019; 30: 2748–2769.
46. Hasheminejad SM and Shabanmotlagh M. Magnetic-field-dependent sound transmission properties of magnetorheological elastomer-based adaptive panels. *Smart Mater Struct* 2010; 19: 035006.
47. Ying ZG, Ni YQ and Ye SQ. Stochastic micro-vibration suppression of a sandwich plate using a magnetorheological visco-elastomer core. *Smart Mater Struct* 2014; 23: 025019.
48. Vemuluri RB, Rajamohan V and Arumugam AB. Dynamic characterization of tapered laminated composite sandwich plates partially treated with magnetorheological elastomer. *J Sandwich Struct Mater* 2018; 20: 308–350.
49. Vemuluri RB, Rajamohan V and Sudhagar PE. Structural optimization of tapered composite sandwich plates partially treated with magnetorheological elastomers. *Compos Struct* 2018; 200: 258–276.
50. Soleymani T and Arani AG. On aeroelastic stability of a Piezo-MRE sandwich plate in supersonic airflow. *Compos Struct* 2019; 230: 111532.
51. Hoseinzadeh M and Rezaeepazhand J. Dynamic stability enhancement of laminated composite sandwich plates

- using smart elastomer layer. *J Sandwich Struct Mater* 2020; 22: 2796–2817.
52. Mead DM. Wave propagation in continuous periodic structures: research contributions from Southampton, 1964–1995. *J Sound Vib* 1996; 190: 495–524.
 53. Hussein MI, Leamy MJ and Ruzzene M. Dynamics of phononic materials and Structures: historical origins, recent progress and Future Outlook. *Appl Mech Rev* 2014; 66: 040802.
 54. Lee SY, Ke HY and Kao MJ. Flexural waves in a periodic beam. *ASME J Appl Mech* 1990; 57: 779–783.
 55. Hawwa MA. Reflection of flexural waves in geometrically periodic beams. *J Sound Vib* 1997; 199: 453–461.
 56. McIntyre JS, Rasmussen ML, Bert CW, et al. Resonance in fiber-reinforced composite materials with sinusoidal stiffness properties. *Wave Motion* 1999; 30: 97–123.
 57. Wierzbicki E and Woźniak C. On the dynamics of combined plane periodic structures. *Arch Appl Mech* 2000; 70: 387–398.
 58. Hvatov A and Sorokin S. Free vibrations of finite periodic structures in pass- and stop-bands of the counterpart infinite waveguides. *J Sound Vib* 2015; 347: 200–217.
 59. Domadiya PG, Manconi E, Vanali M, et al. Numerical and experimental investigation of stop-bands in finite and infinite periodic one-dimensional structures. *J Vib Control* 2016; 22: 920–931.
 60. Ying ZG and Ni YQ. Dynamic characteristics of infinite-length and finite-length rods with high-wave-number periodic parameters. *J Vib Control* 2018; 24: 2344–2358.
 61. Nayfeh AH and Hawwa MA. Use of mode localization in passive control of structural buckling. *AIAA J* 1994; 32: 2131–2133.
 62. Pierre C. Mode localization and eigenvalue loci veering phenomena in disordered structures. *J Sound Vib* 1988; 126: 485–502.
 63. Hunt GW and Wade MA. Localization and mode interaction in sandwich structures. *Proc R Soc London A* 1998; 454: 1197–1216.
 64. Bendiksen OO. Localization phenomena in structural dynamics. *Chaos Solitons Fractals* 2000; 11: 1621–1660.
 65. Cai GQ and Lin YK. Statistical distribution of frequency response in disordered periodic structures. *AIAA J* 1992; 30: 1400–1407.
 66. Bouzit D and Pierre C. Vibration confinement phenomena in disordered, mono-coupled, multi-span beams. *ASME J Vib Acoust* 1992; 114: 521–530.
 67. Cai CW, Cheung YK and Chan HC. Mode localization phenomena in nearly periodic systems. *ASME J Appl Mech* 1995; 62: 141–149.
 68. Elishakoff I, Li YW and Starnes JH Jr. Buckling mode localization in elastic plates due to misplacement in the stiffener location. *Chaos Solitons Fractals* 1995; 5: 1517–1531.
 69. Bardell NS, Langley RS, Dunsdon JM, et al. The effect of period asymmetry on wave propagation in periodic beams. *J Sound Vib* 1996; 197: 427–445.
 70. Xie WC. Buckling mode localization in rib-stiffened plates with randomly misplaced stiffeners. *Comput Struct* 1998; 67: 175–189.
 71. Au FT, Zheng DY and Cheung YK. Vibration and stability of non-uniform beams with abrupt changes of cross-section by using C^1 modified beam vibration functions. *Appl Math Model* 1999; 23: 19–34.
 72. Luongo A. Mode localization in dynamics and buckling of linear imperfect continuous structures. *Nonlinear Dyn* 2001; 25: 133–156.
 73. Ying ZG and Ni YQ. Vibration localization and anti-localization of nonlinear multi-support beams with support periodicity defect. *Symmetry* 2021; 13: 2234.
 74. Shelley FJ and Clark WW. Active mode localization in distributed parameter systems with consideration of limited actuator placement, part 1: theory. *ASME J Vib Acoust* 2000; 122: 160–164.
 75. Michalak B. Vibrations of plates with initial geometrical periodical imperfections interacting with a periodic elastic foundation. *Arch Appl Mech* 2000; 70: 508–518.
 76. Ruzzene M and Baz A. Control of wave propagation in periodic composite rods using shape memory inserts. *ASME J Vib Acoust* 2000; 122: 151–159.
 77. Romeo F and Luongo A. Vibration reduction in piecewise bi-coupled periodic structures. *J Sound Vib* 2003; 268: 601–615.
 78. Wu TY and Wang KW. Periodic isolator design enhancement via vibration confinement through eigenvector assignment and piezoelectric circuitry. *J Vib Control* 2007; 13: 989–1006.
 79. Hull AJ. Dynamic response of an elastic plate containing periodic masses. *J Sound Vib* 2008; 310: 1–20.
 80. Yan ZZ, Zhang C and Wang YS. Attenuation and localization of bending waves in a periodic/disordered fourfold composite beam. *J Sound Vib* 2009; 327: 109–120.
 81. Casadei F, Ruzzene M, Dozio L, et al. Broadband vibration control through periodic arrays of resonant shunts: experimental investigation on plates. *Smart Mater Struct* 2010; 19: 015002.
 82. Claeys CC, Vergote K, Sas P, et al. On the potential of tuned resonators to obtain low-frequency vibrational stop bands in periodic panels. *J Sound Vib* 2013; 332: 1418–1436.
 83. Song Y, Wen J, Yu D, et al. Suppression of vibration and noise radiation in a flexible floating raft system using periodic structures. *J Vib Control* 2015; 21: 217–228.
 84. Chen JS and Tsai SM. Sandwich structures with periodic assemblies on elastic foundation under moving loads. *J Vib Control* 2016; 22: 2519–2529.
 85. Lallart M, Yan L, Richard C, et al. Damping of periodic bending structures featuring nonlinearly interfaced piezoelectric elements. *J Vib Control* 2016; 22: 3930–3941.
 86. Harne RL and Urbanek DC. Enhancing broadband vibration energy suppression using local buckling modes in constrained metamaterials. *ASME J Vib Acoust* 2017; 139: 061004.
 87. Wei J and Petyt M. A method of analyzing finite periodic structures, part 2: comparison with infinite periodic structure theory. *J Sound Vib* 1997; 202: 571–583.
 88. Yeh JY and Chen LW. Wave propagations of a periodic sandwich beam by FEM and the transfer matrix method. *Comput Struct* 2006; 73: 53–60.
 89. Mead DJ. The forced vibration of one-dimensional multi-coupled periodic structures: an application to finite element analysis. *J Sound Vib* 2009; 319: 282–304.
 90. Jędrusiak J. Higher order vibrations of thin periodic plates. *Thin-Walled Struct* 2009; 47: 890–901.
 91. Bisegna P and Caruso G. Dynamical behavior of disordered rotationally periodic structures: a homogenization approach. *J Sound Vib* 2011; 330: 2608–2627.

92. Junyi L and Balint DS. An inverse method to determine the dispersion curves of periodic structures based on wave superposition. *J Sound Vib* 2015; 350: 41–72.
93. Wu ZJ and Li FM. Spectral element method and its application in analysing the vibration band gap properties of two-dimensional square lattices. *J Vib Control* 2016; 22: 710–721.
94. Ying ZG and Ni YQ. A response-adjustable sandwich beam with harmonic distribution parameters under stochastic excitations. *Int J Struct Stab Dyn* 2017; 17: 1750075.
95. Yan MJ and Dowell EH. Governing equations for vibrating constrained-layer damping sandwich plates and beams. *ASME J Appl Mech* 1972; 39: 1041–1046.
96. Mead DJ. The damping properties of elastically supported sandwich plates. *J Sound Vib* 1972; 24: 275–295.